New type of magnetic structure in the R_2T_2X group: Tb_2Pd_2In

Silvie Maskova-Cerna[1], Milan Klicpera[1], Pavel Svoboda[1], Alexander V. Andreev[2], Yurii Skourski[3], Manfred Reehuis[4], Jens-Uwe Hoffmann[4], Gilles Andre[5], Ladislav Havela[1]

[1] Department of Condensed Matter Physics, Charles University, Ke Karlovu 5, 12116 Prague 2, the Czech Republic

[2] Institute of Physics, AVCR, Na Slovance 2, 18221 Prague 8, the Czech Republic

[3] Hochfeld-Magnetlabor, FZ Dresden-Rossendorf, D-01314 Dresden, Germany

[4] Helmholtz-Zentrum Berlin für Materialien und Energy, Hahn-Meitner Platz 1, D-14109 Berlin, Germany

[5] Laboratoire Léon Brillouin, CEA-CNRS, CEA Saclay, 91191 Gif-sur-Yvette Cedex, France

Keywords: intermetallic compounds, magnetic frustration, magnetic properties, single crystal

Abstract

Anisotropy of bulk magnetic properties and magnetic structure studies of a Tb_2Pd_2In single crystal by means of bulk magnetization methods and neutron diffraction techniques confirmed the antiferromagnetic order below the Néel temperature 29.5 K. The collinear magnetic structure of Tb magnetic moments aligned along the tetragonal *c*-axis is characterized by a propagation vector $\boldsymbol{k}$ = (1/4, 1/4, 1/2), yielding an equal-moment-size structure with alternating coupling between nearest as well as next-nearest Tb neighbors within the basal plane and antiferromagnetic coupling between the *c*-axis neighbors. In the context of magnetism of R_2T_2X compounds, where R stands for rare-earth or actinide element, such collinear structure with long-wavelength periodicity represents a new type of magnetic structure.

I. Introduction

A large number of RE_2T_2X compounds (T = transition metal, X = *p*-metal), crystallizing in the Mo_2FeB_2 structure type (space group *P*4/*mbm*. no. 127), is formed both for lanthanides and actinides [1,2], which gives a good opportunity to compare the rare-earth 4*f* magnetism with that related to 5*f* states in actinides. While the actinide-based compounds (studied mainly for U and Np) exhibit a crossover, as the 5*f* hybridization with ligand states gets stronger, from antiferromagnetic order (critical temperatures do not exceed 60 K) to weak Pauli paramagnetism, the ones with regular rare-earths are mostly antiferromagnetic (ferromagnetic ground state appears in few cases [1]), with critical temperatures typically lower than in actinides, despite much larger magnetic moments.

Specific magnetic properties of both actinides and lanthanides are intimately related to details of the crystal structure. The tetragonal Mo_2FeB_2-type structure, representing an ordered ternary derivative of the U_3Si_2 type, consists of two types of basal-plane sheets, which alternate along the *c*-axis. The *f*-atoms are exclusively in one type of the sheet (see Fig.1a,b), and they form there a special triangular motif which, depending on the type of exchange interactions, can bring a geometrical frustration into the system, as it is equivalent to the 2-dimensional Shastry–Sutherland lattice arrangement [3]. The reason is the presence of *f*-*f* dimers with a short *f*-element spacing in the basal plane. An interplay of the specific lattice geometry and multipole interactions was observed in Yb_2Pt_2Pb [4]. Recently, this compound was shown to exhibit exotic magnetic excitations [5].

In general, each *f*-atom has only one nearest neighbor in the basal plane. Besides there are 4 other neighbors little more apart. Adding two more neighbors along the *c*-axis (the distance equal to *c*) leads to a possible complex magnetic phase situation [6]. The variability of the U-U spacings in U_2T_2X compounds, with the shortest U-U links either in the basal plane or along the *c*-axis, allows to test the validity of the two-ion anisotropy mechanism for actinides, confining magnetic moments to a direction perpendicular to the shortest U-U links, e.g. within the basal plane for U_2Pd_2In, which has the shortest U-U spacing along the *c*-axis [7], while the *c*-axis orientation in U_2Ni_2Sn relates to the shortest U-U links in the basal-plane dimers [8].

Beyond the basic characterization, experimental research has to be based on single crystals as necessary prerequisite. The effort to synthesize crystals has been, however, limited to few cases only (mainly with uranium [7,8]). As to RE_2Pd_2In compounds, there was only Ce_2Pd_2In crystal grown, identifying the lack of the Kondo effect, speculated before to co-exist with the ferromagnetism [9]. At present it is rather tempting to study selected isostructural

compounds based on regular rare earths to assess magnetic structures and anisotropy in applied magnetic field so as to confront the 5*f* and 4*f* magnetism. The basic structure and magnetic characterization of the lanthanide-based RE_2Pd_2In series was accomplished by Hulliger and Xue [10]. Their polycrystalline Tb_2Pd_2In was confirmed to crystallize in Mo_2FeB_2-type structure with the lattice parameters a = 7.6595(5) Å, c = 3.7243(4) Å. Its antiferromagnetic ordering temperature of 31 K was the highest among the rare-earth materials. Very similar data, a = 7.6636(2), c = 3.7239(1), T_N = 32 K, were given in later study [11], while ref. [2] gives slightly different numbers, a = 7.6728(2), c = 3.7188(1), T_N = 33 K. Magnetic structure study of a polycrystalline material concluded an antiferromagnetic order with propagation vector $\boldsymbol{k}$ = (1/4,1/4,1/2) and Tb moments aligned along the c-axis below T_N = 33 K [12]. In the present work we report on the synthesis of a Tb_2Pd_2In single crystal and investigation of its low-temperature properties by bulk methods and neutron diffraction.

II. Experimental details

The single crystal of Tb_2Pd_2In used here has been already studied [13]. It had been prepared by the Czochralski growth method using a tri-arc furnace. The crystal growth of this material is rather tricky. As the sample melts incongruently, the formation of single crystal is very sensitive to pulling speed and rotation of both seed and crucible. Sufficiently long time is required to form an ingot. On the other hand, the ingot has a tendency to dissolve in the melt. Indeed, the surface of the ingot reveals an oscillatory behavior of the interface between molten and solid phase, indicating that the heat from the incongruent transition affects the temperature of the melt. Nevertheless, we found that a single crystal can be formed in the core of the ingot, similar to the flux-growth process, if proper parameters are chosen. The optimal pulling speed 6 mm/h, seed rotation 4 RPM with roughly the same counter-rotation of the crucible gave eventually a high-quality single crystalline core surrounded by a soft polycrystalline shell. The crystal of 37 mg (~ 2x2x1 mm^3) was obtained, oriented and used for studies of magnetic properties and neutron diffraction. Another small single crystal of 3.4 mg was extracted for specific heat measurement. The sample was not specially handled as we did not observe any oxidation at ambient conditions on the timescale of years.

The powder X-ray diffraction and Laue X-ray diffraction were employed to determine the crystal structure and quality of the prepared sample.

Quantum Design PPMS equipment was used for magnetic studies and heat-capacity measurements. Magnetic measurements of Tb_2Pd_2In were performed in the temperature range 2-300 K and fields up to 14 T along all principal directions, namely [100] (a-axis), [110] (basal-

plane diagonal), and [001] (*c*-axis), using different orientation of the same crystal. The measurement of magnetization was extended to 60 T using the pulse-field magnet of the Dresden High Magnetic Field Laboratory at Rossendorf. The specific heat was measured on non-oriented single crystal fragment (mass of 3.4 mg) down to 0.4 K using the ^{3}He insert for PPMS.

The magnetic structure was first studied on powder sample using the G4-1, Two-Axis Diffractometer on cold neutron guide G4 in Laboratoire Léon Brillouin, Sacley. The pyrolytic graphite with vertical focusing (neutron wavelength of 2.42 Å), cryofurnace (allowing to cool the sample down to T = 1.7 K) and linear multidetector (800 cells with BF_3 neutron detectors covering 80 degrees in 2θ) were employed to carry out the experiment on a 6 g of powder polycrystalline sample (prepared by arc-melting under Ar atmosphere). Powder neutron diffraction patterns were collected at T = 40 K and 1.7 K.

Single-crystal neutron scattering experiments were carried out at the Helmholtz-Zentrum Berlin. The data were collected on the flat-cone E2 and the four-circle diffractometer E5. The E2 experiment used a standard orange-type cryostat capable to reach base temperature T = 1.5 K. For single-crystal experiment, we used the multi detector bank (four 2D detectors 300x300 mm^2) and the sample table allowing a tilt around an axis perpendicular to the monochromatic beam to investigate upper layers in reciprocal space (Flat-Cone technique). The crystal was mounted within the (1 1 0) - (0 0 1) scattering plane. The E5 diffractometer is equipped with the monochromator with a take-off angle fixed at 42° and two-dimensional position sensitive ^{3}He-detector.

III. Bulk properties

3.1. Single crystal characterization

The Laue X-ray diffraction performed on Tb_2Pd_2In confirmed the prepared ingot to be a single grain crystal with a tetragonal structure. The Laue patterns were taken at various places of the crystal including the reversion of the crystal by 180 degrees between two successive measurements. The single phase neutron-diffraction patterns obtained on E5 were fitted to the model containing the tetragonal ordered Mo_2FeB_2-type structure (space group 127, *P*4/*mbm*), with atomic positions: Tb *4*(*h*) (*x*, *x*+1/2, 1/2), Pd *4*(*g*) (*x*, *x*+1/2, 0), In *2*(*a*) (0,0,0), using the Fullprof program employing the Rietveld analysis [14]. The refined lattice parameters a = 7.670(3) Å and c = 3.720(1) Å) are well in agreement with the data reported previously [2,10,11,13]. No indication of possible off-stoichiometry (incongruent melt during the single

crystal preparation) was found throughout the present study. The internal parameter was determined as $x = 0.1739$. Each Tb atom has one nearest neighbor within the basal plane at d_{a1} = 3.773 Å. 4 more Tb atoms in the basal plane are somewhat more apart (d_{a4} = 4.009 Å). Two more neighbors are located along the *c*-axis at d_{c2} (3.720 Å).

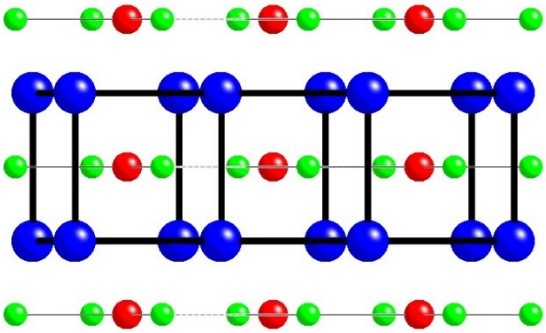

Fig.1a: Projection of the Mo_2FeB_2 structure type along the *a*-axis. Tb, Pd and In atoms are drawn as blue, green and red circles, respectively.

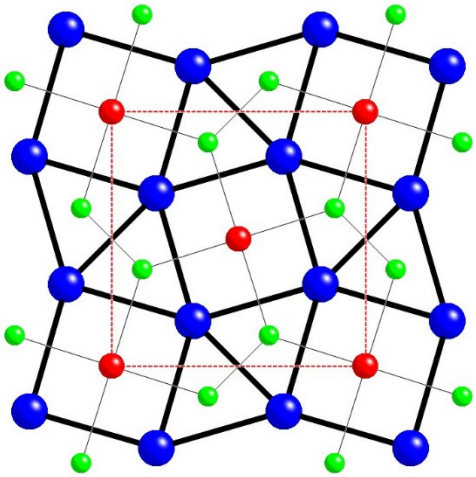

Fig.1b: Projection of the Mo_2FeB_2 structure type along the *c*-axis. Atoms connected by thin lines lie on the planes at $z = 0$ and by thick lines at $z = ½$. The dotted red lines mark the basis of the tetragonal structure.

3.2. Magnetic properties

The temperature dependence of magnetic susceptibility measured along [100] and [001] crystallographic directions indicates a high magneto-crystalline anisotropy in the whole temperature range, the *c*-axis being the easy axis of magnetization [13]. The dependences of the inverse magnetic susceptibility (Fig. 2) along both directions are parallel to each other above 60 K and can be described by the Curie-Weiss law, yielding paramagnetic Curie temperatures θ_p^a = - 46 K and θ_p^c = 3 K, respectively, and the effective magnetic moment μ_{eff} = 10.54 μ_B/Tb. This value is higher than the theoretical one of 9.72 μ_B/Tb^{3+}, which may be ascribed to the polarization of the Tb-5*d* states. The 4*d* band of Pd is likely to be filled and therefore non-magnetic in compounds with strongly electropositive rare earths. Moreover, as the individual effective moments are added as squares into the total effective moment, hypothetical Pd moment of e.g. 1 μ_B would anyway enhance the total μ_{eff} only by 1%.

Weak positive θ_p–value of Tb_2Pd_2In for the susceptibility measured along the *c*-axis indicates ferromagnetic interactions of certain Tb-Tb pairs. The difference to θ_p for fields along *a* and *c* gives the estimate of the energy of magneto-crystalline anisotropy $E_a = k_B\Delta\theta_p \approx 4.2$ meV. For magnetic field along the *c*-axis, $\chi(T)$ in $\mu_0 H = 2$ T starts to deviate from the Curie-Weiss behavior below ≈ 30 K, and this gradual decrease is abruptly interrupted by a drop at $T = 25$ K. For field along the *a*-axis, the deviation from the Curie-Weiss behavior is observed already around 60 K, while the drop at $T = 25$ K manifests a similar behavior as in the $H \parallel c$ case. The temperature of magnetic ordering, $T_N = 29.5$ K, is determined from our specific heat data measured in zero magnetic field (see section 3.3). The measurement of magnetic susceptibility at various magnetic fields showed that T_N decreases with applied field (not shown here), which explains the 4.5 K difference between the drop in susceptibility (in $\mu_0 H = 2$ T) and T_N estimated from the specific heat measured in zero field.

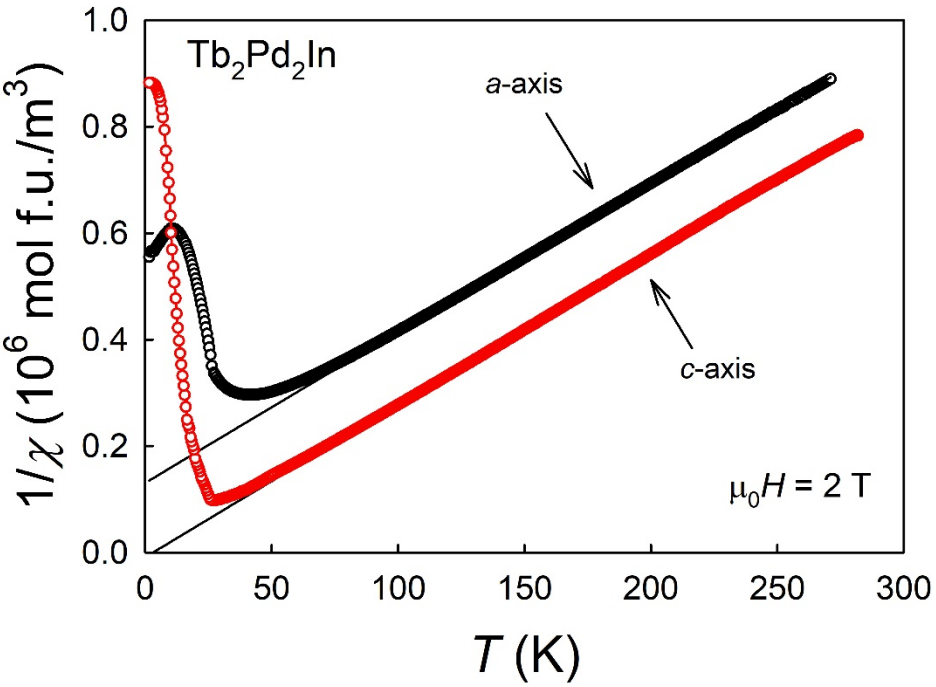

Fig. 2: Temperature dependences of inverse magnetic susceptibility measured along the principal crystallographic axes of Tb_2Pd_2In single crystal in magnetic field $\mu_0 H = 2$ T. The lines represent the Curie-Weiss susceptibility calculated from fitted parameters listed in the text.

Magnetization curves taken at $T = 2$ K (Fig. 3) confirm the high magneto-crystalline anisotropy of Tb_2Pd_2In even within the basal plane of the tetragonal unit cell [13]. The easy-axis magnetization curve exhibits two metamagnetic transitions (probably of spin-flip type)

yielding saturated magnetization 19.1 μ_B/f.u., again slightly more than the full theoretical moment per 2 Tb ions (18 μ_B). The intermediate phase, stable in the field range 6-7 T, exhibits about 50% of the full magnetization. A natural explanation of such intermediate state is that one of 4 antiferromagnetically coupled Tb moments (presumably aligned along the *c*-axis) within one unit cell flips along the field direction. Considering the description of magnetic structure below, this means the transition from (+ - + -) to (+ + + -) arrangement within each unit cell. Such arrangement would naturally break the AF coupling along *c* present in the ground state (see section IV). Concurrently, other explanations of the intermediate state can be introduced, e.g. purely ferromagnetic sheets (+ + + +) interlaced along *c* with original sheets of the (+ - + -) type.

The spin-flip transition for magnetic field applied along *a*, i.e. perpendicular to the easy-magnetization direction, which takes place in significantly higher field of 12-13 T, is rather unusual. A gradual canting of moment, i.e. spin-flop, would be expected as the field rotates the moments out of the easy direction. The magnetization above the transition reaches about 2/3 of the maximum saturated value, indicating another transition may still follow in higher fields. The critical field of the first-order transition for *H*//*a* tends to decrease with increasing temperature. Also its shape changes, reaching the same shape as found in the *c*-direction (2 broad transitions), at approx. $T = 25$ K (Fig. 3).

Confronting the anisotropy energy $E_a \approx 4.2$ meV from the paramagnetic range (calculated from the difference between the paramagnetic Curie temperatures $\theta_p^a = -46$ K and $\theta_p^c = 3$ K, $E_a = k_B * \Delta\theta_p$) with the anisotropy in the ordered state and assuming the ordered moment of Tb, $\mu_{Tb} = 9.0$ μ_B, we can make a following estimate. The magnetic dipole energy in the field of 1 T (Zeeman energy, $E = \mu_0 * \mu * B$) is 0.522 meV. Hence 4.2 meV is close to the potential energy of Tb moments in the field of 11-12 T, indeed not far from the critical metamagnetic field for H // a. We can therefore conclude that the critical field found experimentally is mainly predetermined by the single-site anisotropy of Tb moments.

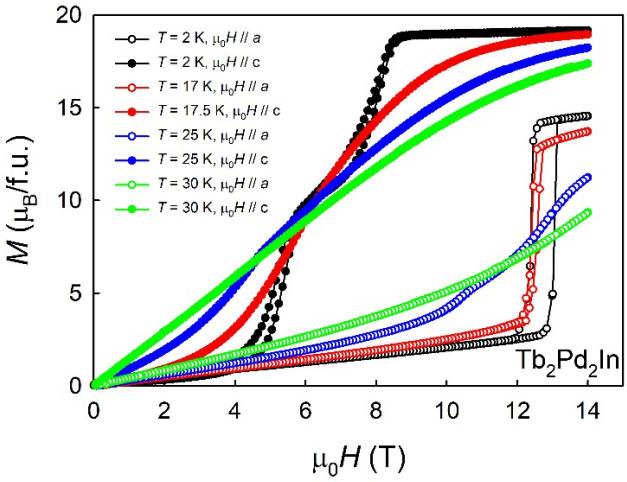

Fig. 3: Magnetization curves of Tb_2Pd_2In measured along principal crystallographic axes at selected temperatures.

The magnetization curve along the [110] direction, which is likely the hardest axis of magnetization, did not exhibit any metamagnetic transition in fields available at PPMS14 (Fig. 4). Nevertheless, taking into account projection from the *a*-axis in the basal plane, such transition was still expected in higher fields. We extended the field range of magnetization measurement employing the pulse-field magnet of the Dresden High Magnetic Field Laboratory at Dresden-Rossendorf (Fig. 5). The measurement indeed revealed the expected metamagnetic transition for H // [110] in $\mu_0 H \approx 15$ T. The magnetization value above the critical field smoothly increases up to 58 T narrowing the difference between H // [100] and H // [110]. No further metamagnetic transition in high magnetic field is observed on [110] data, neither on [100] data. Following our assumption on magnetic moment direction development in magnetic field, following scenario can be constructed: The magnetic field - of 12-13 T and 15 T applied along [100] and [110], respectively - causes a flip of magnetic moments from the *c* direction. However, the field induced directions of individual magnetic moments are not aligned perfectly along the magnetic field direction. (Here we can speculate on exotic magnetic structures of e.g. conical type.) Therefore the total magnetic moment is significantly smaller than the one observed for field applied along the *c*-axis. Further increase of magnetic field aligns the individual magnetic moments progressively along the field direction. Finally, in high magnetic field (> 58 T), polarized ferromagnetic state is attained not only for H // [001] (already in 9 T), but also for H perpendicular to [001]. Alternatively, the magnetic moments are aligned by applied magnetic field along its direction already in 12-13 T (15 T) and with further increase

of field the moment value increases up to the maximal one (as observed for field applied along the easy magnetization axis).

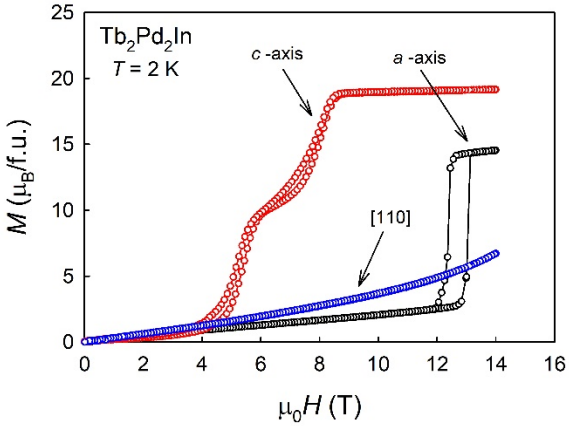

Fig. 4: Magnetization curves of Tb_2Pd_2In measured along principal crystallographic axes at $T = 2$ K.

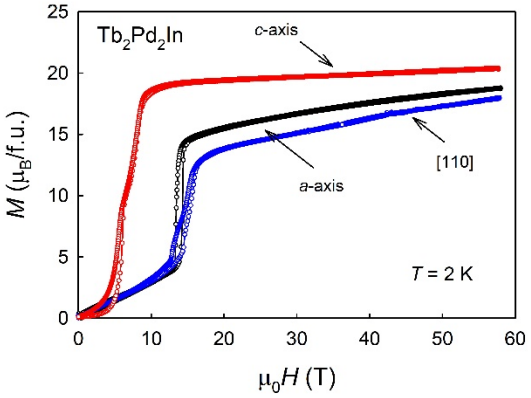

Fig. 5: Magnetization curves of Tb_2Pd_2In measured along principal crystallographic axes in pulsed magnetic field.

3.3. Specific heat

The temperature dependence of specific heat, $C_p(T)$, shows a sharp peak at $T = 29.5$ K, which can be associated with T_N. At high temperatures, $C_p(T)$ can be approximated by a Debye-type lattice contribution and electron contribution with parameters $\Theta_D = 150$ K and $\gamma = 95$ mJ/mol f.u. K^2. However, for a more precise determination of magnetic entropy, S_m, of Tb_2Pd_2In we can use the non-magnetic analogue La_2Pd_2In [14] (Fig. 6). Due to significantly different atomic mass of La and Tb, the La_2Pd_2In data (Sommerfeld coefficient $\gamma = 8$ mJ/mol K^2 [14]) show a lower value of specific heat even at high temperature. To better estimate the magnetic contribution to specific heat, C_m, in Tb_2Pd_2In (subtracting the electronic and lattice contributions) the value of 120 mJ/mol K^2 was added to the specific heat of La_2Pd_2In. The reason for this particular value is in the fact that the high-temperature specific heat data of both compounds practically overlap, as seen in Fig. 6. The shift is rather large and we cannot exclude that it actually includes part of the high temperature magnetic entropy, present due to excitations into high-energy CEF levels. The calculated magnetic contribution C_m to specific heat (obtained by subtracting the non-magnetic analogue) as well as magnetic entropy

($\int \frac{Cm}{T} dT$, i.e the area below the "magnetic" peak) hence represent a low estimate of C_m and S_m of Tb_2Pd_2In.

The entropy S_m estimated per one Tb atom (1 formula unit contains 2 Tb atoms) is close to R*ln2 at T_N (Fig. 7). As the total magnetic entropy has to reach R*ln(13), expected for the full multiplicity of the 4*f* state with orbital momentum $J = 6$, a large amount of magnetic entropy has to be located above T_N . Besides e.g. with short-range correlations, which can reflect in entropy close above T_N, higher CEF levels have to be populated in this temperature range. At very low temperatures (below $T = 2$ K) a large nuclear contribution of Tb [15] yields a pronounced upturn in $C_p(T)$ (Inset of Fig. 6). This situation prohibits us to perform a quantitative analysis of $C_p(T)$ in the ordered state.

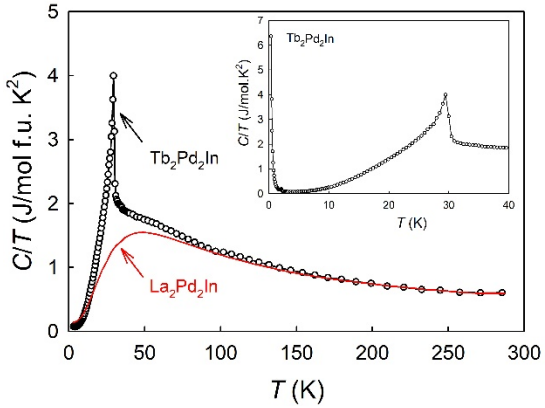

Fig. 6: The temperature dependence of the specific heat (in the C/T vs. T representation) for Tb_2Pd_2In single crystal compared to La_2Pd_2In [14]. The La_2Pd_2In data were shifted by 120 mJ/mol K^2. See details in text. The inset shows the detail of the temperature dependence of the specific heat (in the C/T vs. T representation) for Tb_2Pd_2In single crystal.

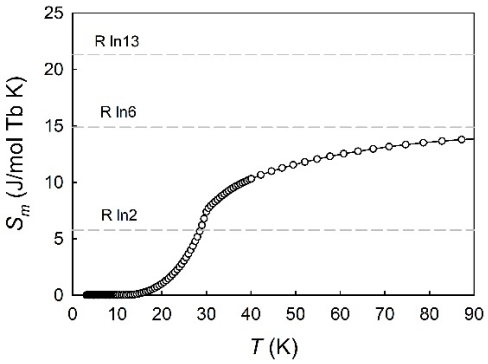

Fig. 7: The magnetic entropy change ΔS per one Tb atom estimated using the non-magnetic analogue La_2Pd_2In [14].

IV. Magnetic structure

4.1. Powder neutron diffraction

The refinement of powder neutron diffraction data measured in the low-temperature region confirmed Tb_2Pd_2In crystallizing in the Mo_2FeB_2-type structure (space group 127,

*P*4/*mbm*). Refined lattice parameters $a = 7.626(3)$ Å and $c = 3.712(1)$ Å from $T = 40$ K powder patterns are well in agreement with X-ray diffraction results (room temperature data only).

Comparing the diffraction patterns measured at 40 K and 1.7 K, i.e. in the paramagnetic and ordered state, respectively, a number of clear magnetic peaks (at least 12 high-intensity peaks) can be identified besides the nuclear reflections. Observed magnetic reflections can be fully described by propagation vector $k = (1/4, 1/4, 1/2)$ in a good agreement with previous study [11].

The knowledge on both crystal structure and propagation vector allows us to calculate possible magnetic structures by performing a symmetry analysis employing the program BasIreps [16]. The symmetry calculations bring following information on magnetic structure: (1) Considering the given propagation vector *k*, four possible one-dimensional irreducible representations are obtained: $\Gamma_1(1, i, 1, i)$, $\Gamma_2(1, i, -1, -i)$, $\Gamma_3(1, -i, 1, -i)$ and $\Gamma_4(1, -i, -1, i)$; the order of symmetry operators is 1, 2_{xx}, m_{xy} and n_{xxz}. (2) The propagation vector *k* is not equivalent to *–k*. Therefore, both propagation vectors have to be considered during the data refinement. The vector star is formed by four vectors. (3) Terbium 4*h* site decomposes into three orbits: Tb_1, Tb_2 and Tb_3, where the last orbit splits into two $Tb_{3\text{-}1}$ and $Tb_{3\text{-}2}$. Obtained basis functions dictate the magnetic moments to be aligned either within the basal plane (Γ_1 and Γ_3) or along the *c*-axis (Γ_2 and Γ_4).

The refinement of neutron diffraction data using model magnetic structures as obtained by representation analysis resulted into a good agreement between data and fit for $\Gamma_2(1, i, -1, -i)$ with generally complex Fourier coefficients for Tb orbits $S_1 = (0, 0, u)$, $S_2 = (0, 0, u)$, $S_{3\text{-}1} = (0, 0, u)$ and $S_{3\text{-}2} = i(0, 0, u)$. The magnetic structure with moments aligned along the *c*-axis is in excellent agreement with suggestions of the previous study [11].

Taking into account the commensurate propagation vector, the magnetic space group can be found for refined magnetic structure (program MaxMagn [17]): from 8 maximal magnetic subgroups of paramagnetic *P*4/*mbm* the best agreement was achieved for the group C_amca. The phase between different Fourier components of the magnetic moments cannot be determined unambiguously by diffraction methods. Symmetry constraints and, more importantly, restrictions on the amplitude of the magnetic moments can reduce the number of solutions [18]. The maximum value of magnetic moment on Tb is restricted by value of the magnetic moment of the Tb^{3+} free ion, i.e. 9 μ_B. Despite the fact that the phase of individual orbits is not coupled by the symmetry, the best agreement is found for orbits 1 and 2 having the same phase and both positions of the orbit 3, i.e. $Tb_{3\text{-}1}$ and $Tb_{3\text{-}2}$, having the same phase. The mutual phase shift between these pairs of orbits should be 1/4. Taking into account the restriction on size of magnetic moments, the phase of the first pair can be estimated as 3/8 and

the second one as 1/8, leading to magnetic moments $\mu \approx 8.7\ \mu_B$. The magnetic moments on individual orbits are again not restricted by the symmetry, however they tend to have similar value. Considering the same amplitude of magnetic moments, the agreement between the model and data is not significantly worse - the obtained magnetic agreement factor is 3.5% compared to 3.3% for unrestricted, but in reality only slightly different, moments on different orbits. Furthermore, a refinement of phases, preserving the same phase for individual pairs of orbits and considering the maximum value of the magnetic moments as 9 μ_B, leads to the agreement factor 3.2%. Any tilt of magnetic moments from the *c*-axis direction does not improve the fit. Figure 8 contains both measured diffraction patterns and corresponding fit to the model of nuclear and magnetic structure. The refined magnetic structure is visualized in Fig. 9. From the above mentioned facts we can take the equal-moment antiferromagnetic structure as most plausible.

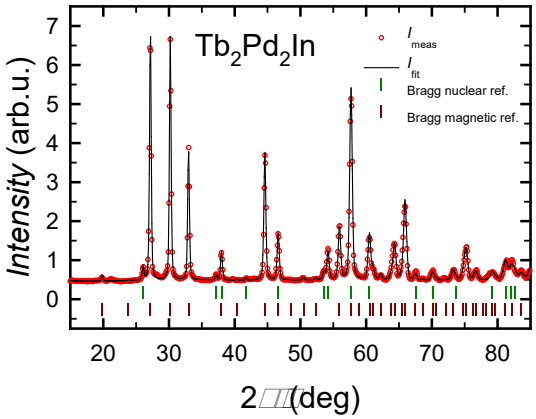

Fig. 8: Powder neutron diffraction patterns of Tb_2Pd_2In measured at 1.7 K employing diffractometer G4-1. Full line represents the model fit done using the FullProf program [16]. Tick marks denote the positions of nuclear (green) and magnetic (dark red) Bragg reflections.

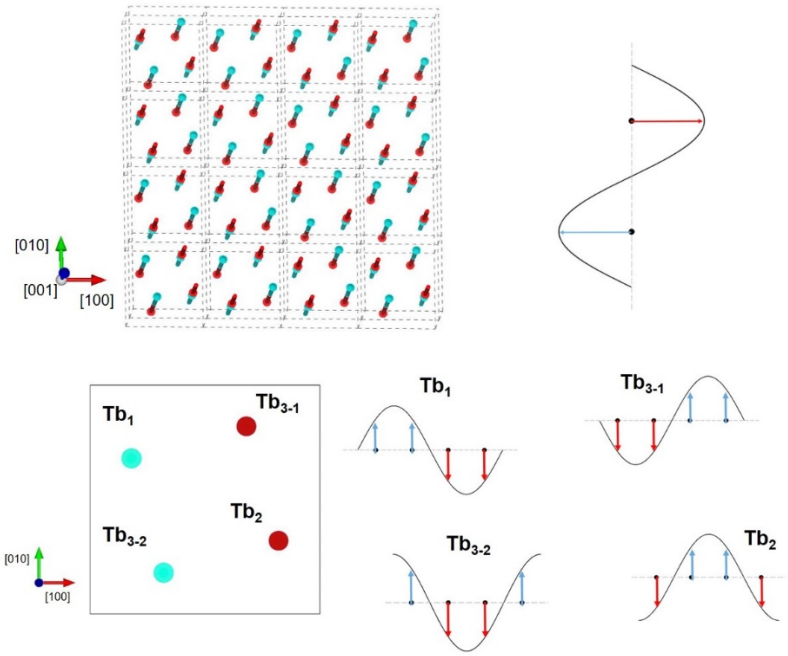

Fig. 9: Schematic view of the magnetic unit cell of Tb_2Pd_2In along direction close to the *c*-axis (upper left), magnetic-moment propagation along the *c*-axis [001] - the arrows show only the amplitude not the moment direction - (upper right) and the propagation of 4 individual magnetic moments from the crystallographic unit cell along the *x*-axis [100] (lower panel). The *y*-axis [010] propagation is equivalent.

4.2. Single-crystal neutron diffraction

The E2 experiment has confirmed the high quality of the single crystal (see Fig. 10) as well as the magnetic structure of Tb_2Pd_2In being described by the propagation vector $\boldsymbol{k}$ = (1/4, 1/4, 1/2) and magnetic moments parallel to the crystallographic *c*-axis. The diffraction pattern remains invariable in the whole temperature range of antiferromagnetic ordering. Unfortunately, based on E2 data we were not able to exclude the presence of possible higher harmonics. Therefore additional diffraction experiment at E5 employing four-circle goniometer was performed.

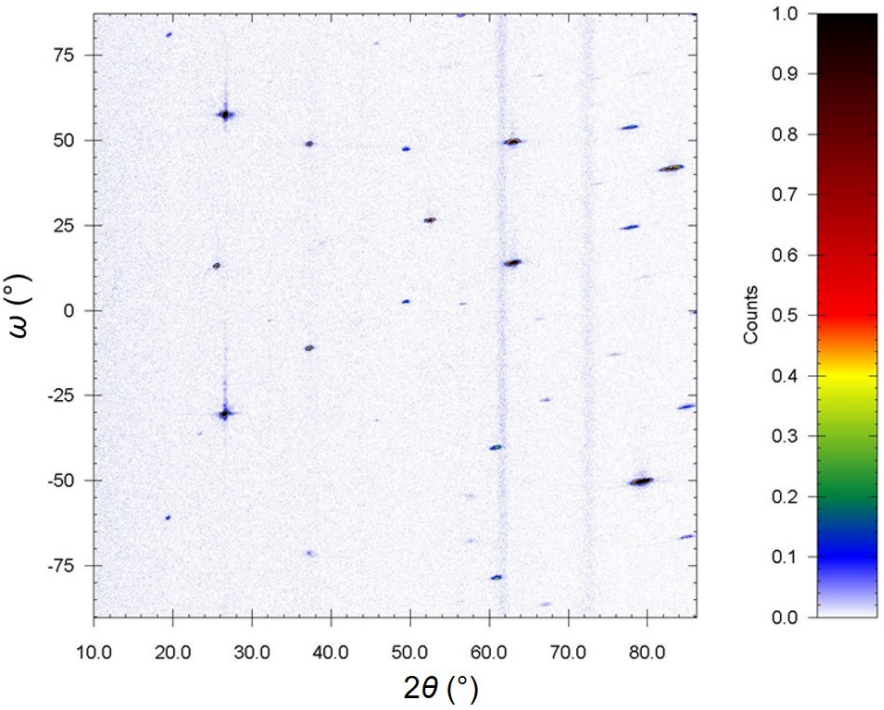

Fig. 10: The diffraction pattern of the Tb_2Pd_2In for λ = 2.4 Å at T = 2 K shows a high quality of the single crystal.

The single crystal experiment led to similar type of conclusions as obtained by the powder neutron diffraction. The magnetic structure is described by the propagation vector of k = (1/4,1/4,1/2) and magnetic moments coupled antiferromagnetically along the c-axis. Although not restricted by the symmetry the magnetic moments on all Tb sites tend to have a same value. Tb_1 and Tb_2 positions and $Tb_{3\text{-}1}$ and $Tb_{3\text{-}2}$ positions can be paired, the moments within the pairs having the same phase. As the diffraction peaks show no additional odd-harmonic intensities, the sinusoidal modulation of the magnetic structure was confirmed.

V. Discussion and conclusions

The present study on a Tb_2Pd_2In single crystal confirmed previous results obtained on the polycrystalline samples [12], and simultaneously brought a new insight into the magnetic structure and behavior in external magnetic fields. The magnetic structure below the Néel transition at T_N = 29.5 K is characterized as an equal-moment structure with moments antiferromagnetically aligned along the c-axis. Their mutual orientation can be described by a single propagation vector $\boldsymbol{k}$ = (1/4, 1/4, 1/2). Hence the coupling within the Tb-Tb pair along c (d_c = 3.720 Å), which is the shortest Tb-Tb distance, is always antiferromagnetic. The coupling

within the basal plane, corresponding to the Tb-Tb dimers, d_{a1} = 3.773 Å, is variable, with 50% pairs coupled ferromagnetically and 50% coupled antiferromagnetically (Fig. 11). The same alternating coupling exists for the next nearest 4 neighbors in the basal plane (d_{a2} = 4.009 Å).

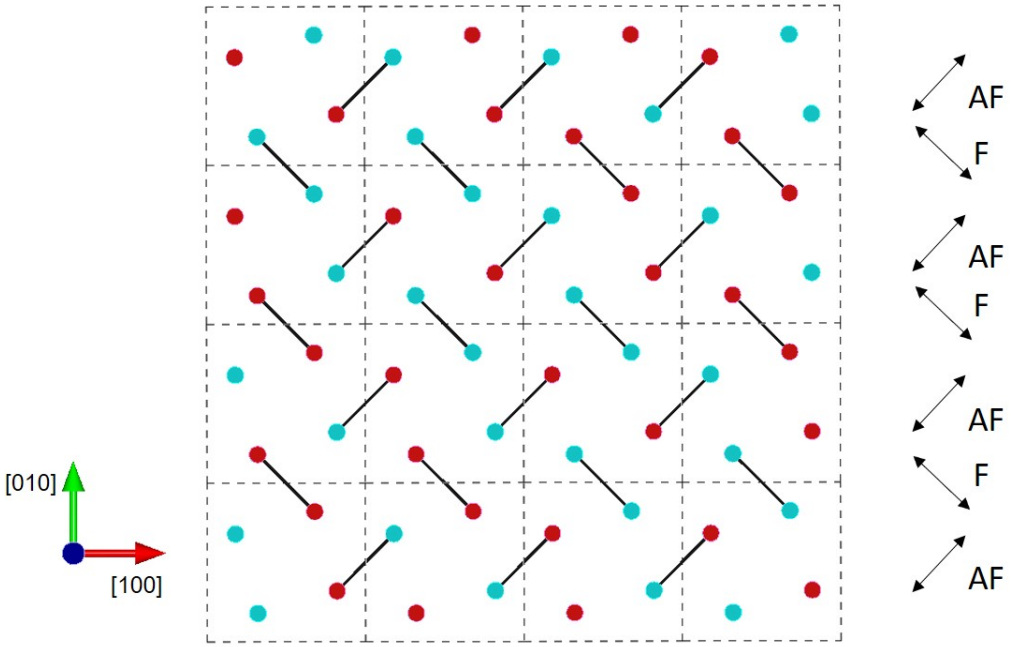

Fig. 11: The coupling of Tb-Tb dimers within the basal plane of Tb_2Pd_2In. The dashed lines represent individual crystallographic unit cells. Tb moments oriented up and down are distinguished by the color as in Fig. 10.

Hence we have to conclude that the type of coupling in Tb_2Pd_2In does not depend on the distance (being the same for both F and AF), but is prescribed by the particular propagation vector ***k***. In other words, the coupling between individual Tb atoms in neighbor unit cells within the basal plane can be characterized as (++--) both along [100] and [010], but this simple pattern imposes a mixed F-AF coupling between nearest neighbors within each unit cell. Such situation can be ascribed to competing F and AF pair interactions, which are obeying requirements of the translation 3D periodicity imposed via the RKKY interaction, depending on non-*f* electrons and the properties of the Fermi surface. The advantage of the given magnetic structure is that despite the long-wavelength periodicity and purely harmonic modulation it is an equal-moment collinear structure. This points to importance of magnetic anisotropy in the system. CEF effects force the moments into the *c*-axis direction. The uniaxial single-ion anisotropy energy forcing the Tb moments into *c* can be estimated as ≈ 4.2 meV.

The AF coupling can be broken either in a two-stage metamagnetic (spin-flip) process with critical fields 5 and 8 T applied along *c* or applying field along the basal plane. Here the [1 0 0] and [1 1 0] directions are inequivalent. The first-order metamagnetic processes for fields along the *ab*-plane mean that the magnetic anisotropy or exchange energy is not monotonously increasing as a function of the angle of moments from the *c*-axis. The determination of variations on magnetic structure in magnetic fields remains an important task.

Tb_2Pd_2In represents, with its *c*-axis orientation of magnetic moments, rather rare case. As we see, the price the system pays for a collinear magnetic structure, required by magnetic anisotropy, is uneasy optimization of exchange interactions, depending on the specific lattice geometry of the Tb_2Pd_2In structure type. The different types of inter-site exchange coupling for equally distant neighbors is a sign of difficult minimization of its total energy. From the other side, the relatively high ordering temperature (highest among all other RE_2Pd_2In materials [11]) does not allow to refer to any real frustrated interactions. The same or similar magnetic structure was reported on the basis of neutron powder diffraction data also for Ho_2Pd_2In [12]. The *c*-axis orientation of magnetic moments was found also for ferromagnetic Ce_2Pd_2In [9]. From other rare-earth based compounds, Nd_2Ni_2In has the Nd moments ordered in a non-collinear pattern in the basal plane, however, the *c*-axis orientation can be achieved in rather low magnetic fields [19,20]. The basal-plane orientation appears also in Yb-containing compounds [4,5]. It would be interesting to have more of the isotypes prepared as single crystals.

For U-based isotypes, the *c*-axis orientation of magnetic moments within the magnetic structure appears only seldom, which can be associated with different anisotropy mechanism. The two-ion interaction of bonding 5*f* states, tends to orient due to strong spin-orbit interaction perpendicular to strong bonding directions, and non-collinear arrangement of U moments in the basal plane comes out in most of the cases as a natural solution. Few exceptions include U_2Ni_2Sn with rather compressed basal plane and elongated *c*-axis [8], and U_2Rh_2Sn [21,22].

A direct comparison can be made with U_2Pd_2In, which belongs to the type with basal-plane orientation of U moments [23,7]. Its Néel temperature T_N = 37 K is not markedly higher than that of Tb_2Pd_2In, but one has to consider much higher spin moment of Tb. Uranium should be rather compared with Nd with $4f^3$ state. Indeed, Nd_2Pd_2In has T_N = 6 K. [11], which demonstrates that the indirect RKKY interaction of rare earths is much weaker than exchange interactions based on the bonding 5*f* states of U.

Acknowledgements

This work was partially supported by the Czech Science Foundation under the grant No. 19-00925S. We acknowledge the support of HLD at HZDR (member of the European Magnetic Field Laboratory) and the Materials Growth and Measurement Laboratory (https://mgml.eu) which is supported within the program of Czech Research Infrastructures (project no. LM2018096). We thank HZB for the allocation of neutron radiation beamtime.

References

[1] M. Lukachuk, R. Pöttgen: Intermetallic compounds with ordered U_3Si_2 or Zr_3Al_2 type structure – crystal chemistry, chemical bonding and physical properties, *Z. Kristallogr.* 218 (2003) 767-787.

[2] S. Mašková, A. Kolomiets, L. Havela, A.V. Andreev, P. Svoboda: Impact of hydrogen absorption on crystal structure and magnetic properties of R_2T_2X compounds, *J. Alloys Compd*. 645 (2015) S76-S79. [3] B. Shastry, B. Sutherland: Exact Ground State of a Quantum Mechanical Antiferromagnet, *Physica* B+C 108 (1981) 1069-1070.

[4] Y. Shimura, T. Sakakibara, K. Iwakawa, K. Sugiyama, and Y. Onuki: Low Temperature Magnetization of Yb_2Pt_2Pb with the Shastry–Sutherland Type Lattice and a High-Rank Multipole Interaction, *J. Phys. Soc. Japan* 81 (2012) 103601.

[5] L.S. Wu, W.J. Gannon, A.I. Zaliznyak, A.M. Tsvelik, M. Brockmann, J.S. Caux, M.S. Kim, Y. Qiu, J.R.D. Copley, G. Ehlers, A. Podlesnyak, M.C. Aronson: Orbital-exchange and fractional quantum number excitations in an *f*-electron metal, Yb_2Pt_2Pb, *SCIENCE* Vol. 352, Issue 6290 (2016) pp. 1206-1210.

[6] S. Bordere, F. Bourée, B. Chevalier, J. Etourneau, Magnetic ground states of the tetragonal U_2Fe_2Sn-type structure using an anisotropic RKKY exchange modeling, *J. Magn. Magn. Mater.* 253 (2002) 15–24.

[7] K. Prokes, H. Nakotte, L. Havela, V. Sechovsky, L.C.J. Pereira, C. Rijkeboer, A. Seret, J.C. Spirlet, P. Svoboda, and F.R. de Boer: Magnetic Anisotropy of U_2Pd_2In, *Physica* B 223-224 (1996) 225-227.

[8] S. Mašková, A.V. Andreev, Y. Skourski, S. Yasin, D.I. Gorbunov, S. Zherlitsyn, H. Nakotte, K. Kothapalli, F. Nasreen, C. Cupp, H. B. Cao, A. Kolomiets, and L. Havela: U_2Ni_2Sn and the origin of magnetic anisotropy in uranium compounds, *Phys. Rev. B* 99 (2019) 064415.

[9] M. Klicpera, S. Maskova, M. Divis, P. Javorsky, L. Havela: Magnetic properties of Czochralski-grown Ce_2Pd_2In single crystal, *J. Magn. Magn. Mater.* 404 (2016) 250-256.

[10] F. Hulliger and B.Z. Xue: On new Mo_2FeB_2-type representatives M_2Pd_2In, *J. Alloys Compd.* 215 (1994) 267-270.

[11] M. Giovannini, H. Michor, E. Bauer, G. Hilscher, P. Rogl, and R. Ferro: Structural chemistry, magnetism and thermodynamic properties of R_2Pd_2In, *J. Alloys Compd.* 280 (1998) 26-38.

[12] T. Herrmannsdorfer, P. Fischer, G. Bottger, L. Keller, M. Giovannini, E. Bauer, Magnetic ordering in the rare-earth intermetallic compounds Tb_2Pd_2In and Ho_2Pd_2In, *Physica* B 276-278 (2000) 702-703.

[13] S. Maskova, A. Kolomiets, L. Havela, A.V. Andreev, P. Svoboda, Y. Skourski: Magnetic properties of Tb_2Pd_2In: single crystal study, *Solid State Phenomena* 194 (2013) 58-61.

[14] A.V. Kolomiets, S. Mašková, L. Havela, Z. Matěj, R. Kužel: Effect of hydrogenation on the crystal structure of La_2Pd_2In, *J. Alloys Compd.* 501 (2011) 4185-4189.

[15] K. Satoh, Y. Fujima, I. Umehara, J. Itoh, Y. Onuki and M. Kasaya: Low-temperature specific heat of RIn_3 (R = La-Ho), *Physica* B 186-188 (1993) 658-660.

[16] J. Rodriguez-Carvajal: Recent developments of the program FULLPROF, *Comm. Powder Diffr. IUCr Newsl*. 26 (2001) 12–19.

[17] J.M. Perez-Mato, S.V. Gallego, E.S. Tasci, L. Elcoro, G. De la Flor, M.I. Aroyo: Symmetry-Based Computational Tools for Magnetic Crystallography; *Annu. Rev. Mater. Res.* 45 (2015) 13.1-13.32.

[18] J. Rodríguez-Carvajal and F. Bourée: Symmetry and magnetic structures, *EPJWeb Conf.* 22 (2012) 00010.

[19] S. Mašková, L. Havela, S. Daniš, A. Llobet, H. Nakotte, K. Kothapalli, R. Černý, A. Kolomiets: Impact of hydrogen absorption on crystal structure and magnetic properties of geometrically frustrated Nd_2Ni_2In, *J. Alloys Compd.* 566 (2013) 22-30.

[20] S. Mašková, S. Daniš, A. Llobet, H. Nakotte, L. Havela: Large Magnetocaloric Effect in Nd_2Ni_2In, *Acta Phys. Polonica* A 126 (2014) 282-283

[21] H. Nakotte, A. Purwanto, R.A. Robinson, L. Havela, V. Sechovsky, L.J.C. Pereira, A. Seret, J. Rebizant, J.C. Spirlet, and F. Trouw: Hybridization Effects in U_2T_2X Compounds: Magnetic Structures of U_2Rh_2Sn and U_2Ni_2In, *Phys. Rev. B* 53 (1996) 3263-3271.

[22] K. Prokes, D.I. Gorbunov, M. Reehuis, B. Klemke, A. Gukasov, K. Uhlirova, X. Fabrèges, Y. Skourski, F. Yokaichiya, S. Hartwig, and A.V. Andreev: Anisotropic physical properties of single-crystal U_2Rh_2Sn in high magnetic fields, *Phys. Rev. B* 95 (2017) 174433.

[23] A. Purwanto, R.A. Robinson, L. Havela, V. Sechovsky, P. Svoboda, H. Nakotte, K. Prokes, F.R. de Boer, A. Seret, J.M. Winand, J. Rebizant, and J. C. Spirlet: Magnetic Ordering in U_2Pd_2In and U_2Pd_2Sn, *Phys. Rev. B* 50 (1994) 6792-6801.